Methylation of Ribosomal Protein L42 Regulates Ribosomal Function and Stress-adapted Cell Growth*⬚

Atsuko Shirai[‡1], **Mahito Sadaie**[‡§1], **Kaori Shinmyozu**[¶], **and Jun-ichi Nakayama**[‡2]

From the ‡*Laboratory for Chromatin Dynamics and* ¶*Proteomics Support Unit, RIKEN Center for Developmental Biology, Kobe 650-0047, Japan and the* §*Cambridge Research Institute, Cancer Research UK, Robinson Way, Cambridge CB2 0RE, United Kingdom*

Lysine methylation is one of the most common protein modifications. Although lysine methylation of histones has been extensively studied and linked to gene regulation, that of non-histone proteins remains incompletely understood. Here, we show a novel regulatory role of ribosomal protein methylation. Using an *in vitro* methyltransferase assay, we found that *Schizosaccharomyces pombe* Set13, a SET domain protein encoded by *SPAC688.14*, specifically methylates lysine 55 of ribosomal protein L42 (Rpl42). Mass spectrometric analysis revealed that endogenous Rpl42 is monomethylated at lysine 55 in wild-type *S. pombe* cells and that the methylation is lost in Δ*set13* mutant cells. Δ*set13* and Rpl42 methylation-deficient mutant *S. pombe* cells showed higher cycloheximide sensitivity and defects in stress-responsive growth control compared with wild type. Genetic analyses suggested that the abnormal growth phenotype was distinct from the conserved stress-responsive pathway that modulates translation initiation. Furthermore, the Rpl42 methylation-deficient mutant cells showed a reduced ability to survive after entering stationary phase. These results suggest that Rpl42 methylation plays direct roles in ribosomal function and cell proliferation control independently of the general stress-response pathway.

Post-translational modifications regulate protein structure and function, and one of the most common is lysine methylation (1). Although lysine methylation does not change the overall charge of the side chain, it can influence the activity of protein by providing a novel interface for its interactions with other molecules. Most protein lysine methylations, with a few exceptions, are catalyzed by the SET domain-containing protein (SET protein) family (2). The SET domain was originally identified in three *Drosophila* proteins, Su(var)3–9, Enhancer of zest, and Trithorax, and was later demonstrated to be the responsible domain for histone-lysine methyltransferase function (3). The characterization of these enzymes has revealed the roles of histone lysine methylation in many different biological processes, including higher order chromatin assembly and transcriptional regulation (4). Recent studies have shown that histone lysine methylation is directly reversed by several histone demethylase families (5).

Lysine methylation has also been identified in non-histone proteins that include ribulose 1,5-bisphosphate carboxylase/oxygenase in plants (6), cytochrome *c* in yeast (7), mammalian TAF10 and p53 (8–10), and ribosomal proteins in a diverse range of species (11). The methylation of ribosomal proteins has been observed in both prokaryotes and eukaryotes. In the budding yeast *Saccharomyces cerevisiae*, a combination of *in vivo* labeling and direct mass spectrometric analysis of the ribosomal proteins revealed that six of them, Rpl1, Rpl3, Rpl12, Rpl23, Rpl42, and Rpl43, are post-translationally methylated (12, 13). By analyzing the methylation state of *S. cerevisiae* mutant strains with deletions in candidate SET domain-containing genes, two SET proteins, Rkm1 and Rkm2, were identified as specific methyltransferases responsible for the dimethylation of Lys-105 and Lys-109 in Rpl23 and the trimethylation of Lys-3 in Rpl12 (14, 15), respectively. A recent study further demonstrated that the monomethylation at Lys-40 and Lys-55 in Rpl42 is dependent on two other SET proteins, the Ybr030w gene product and Set7, respectively (16), although the direct enzymatic activity of these proteins has yet to be demonstrated. Several mass spectrometric studies have also identified methyl modifications on ribosomal proteins in plants and mammals (17–19). Although ribosomal protein methylation appears to be conserved among different organisms, the physiological roles of these lysine methylations remain to be fully elucidated.

The ribosome plays a central role in the adaptation of a cell to environmental stress, as a checkpoint for sensing shifts in temperature and nutrient levels (20, 21). Global translation is reduced in response to these cellular stresses by triggering the phosphorylation of the eukaryotic initiation factor 2α (eIF2α) (22, 23). This prevents the formation of the eIF2-methionine-initiator tRNA (Met-tRNA$_i^{Met}$)-GTP ternary complex and thus blocks translational initiation. The stress-induced attenuation of global translation is often accompanied by the selective translation of proteins that are required for cell survival under stress. A downshift in temperature, one of the most common environmental changes for microbial life, induces the expression of genes encoding a number of ribosomal proteins and proteins involved in ribosome biogenesis and assembly (24). Thus, it has been suggested that cells remodel the translational machinery and secondary structure of RNA for cold growth. Interestingly, ribosomal protein biogenesis and the stress-responsive signaling pathway are also linked with the life span in both yeast and *Caenorhabditis elegans* (25–28).

[1] Supported by a Special Postdoctoral Researchers Program of RIKEN. Both authors contributed equally to this work.
[2] To whom correspondence should be addressed: RIKEN Center for Developmental Biology, 2-2-3 Minatojima-minamimachi, Chuo-ku, Kobe, Hyogo 650-0047, Japan. Tel.: 81-78-306-3205; Fax: 81-78-306-3208; E-mail: jnakayam@cdb.riken.jp.

In the fission yeast *Schizosaccharomyces pombe*, 13 SET proteins have been identified in the genome, four of which (Set1, Set2, Clr4, and Set9) are histone-lysine methyltransferases and involved in transcriptional regulation (29–32). Using an *in vitro* methyltransferase assay and genome-wide screen for methylated proteins, we previously demonstrated that Set5, Set10, and Set11 are specific methyltransferases for EF1α, Rpl23, and Rpl12, respectively (33, 34). However, the roles played by other SET proteins in cellular processes and their physiological substrates remain unresolved.

In this study, we show that *S. pombe* Set13, a SET protein encoded by *SPAC688.14*, is a specific methyltransferase responsible for monomethylation at lysine 55 in Rpl42. We further demonstrate that this methyl modification is highly conserved from yeast to humans. Rpl42 methylation-deficient mutant *S. pombe* cells showed defects in stress-adapted growth control and reduced survival potential. Notably, Rpl42 methylation-mediated stress adaptation occurred independently of the general stress-response pathway. These results suggested that this ribosomal protein methylation is involved in global ribosomal function and cellular growth control.

EXPERIMENTAL PROCEDURES

Strains and Media—The strains used in this study are listed in supplemental Table S4. All of the yeast strains were grown at 30 °C or the indicated temperature in YEA (0.5% yeast extract, 3% glucose, 75 μg/ml adenine) or minimal medium (SD or EMM) supplemented with amino acids for auxotrophic markers and antibiotics. The deletion and tagging of endogenous genes were conducted using a PCR-based gene-targeting protocol (35). The deletion mutants for the *set13+*, *gcn5+*, or *gcn2+* gene were made by replacing the gene with a *kan^r* or *ura4+* marker gene. The integrated *ura4+* gene was then removed by homologous recombination of the flanking *TEF* terminator sequences to obtain cells lacking it. To obtain the *rpl42^K55R* and *rpl42^P56Q* mutant strains, the *rpl42+* coding sequence was first cloned into pCRII-TOPO (Invitrogen), and each mutation was introduced by site-directed mutagenesis. After insertion of the *ura4+* marker gene, the resultant plasmids were digested with MfeI and used to transform cells. Cells in which the plasmid was introduced into the original *rpl42+* locus were isolated as *ura4+*-expressing cells. The mutant *S. pombe* strains that lost the wild-type *rpl42+* allele and *ura4+* gene by internal homologous recombination were isolated using counter-selective media containing 5-fluoroorotic acid.

To obtain *S. pombe* cells expressing EGFP[3]-fused Set13, the *set13+* coding sequence was cloned into pREP1-EGFP, a pREP1 derivative containing the EGFP-coding sequence (36), and cells transformed with the resulting plasmid were isolated with minimal medium lacking leucine. To express EGFP-fused Rpl42, the *rpl42+* coding sequence previously isolated as part of the ORFeome project (37) was transferred to a pDUAL-GFH1c vector (38) by the "LR" recombination reaction. The resultant

plasmid, pDUAL-GFH1-*rpl42*, was digested with NotI and introduced into the *leu1* locus of wild-type or Δ*set13* cells. The transformed cells were selected on SD lacking leucine.

Expression and Purification of Recombinant Proteins—To produce recombinant Set13 or Rpl42 proteins in *Escherichia coli*, the coding sequence for *set13+* or *rpl42+* was amplified by PCR and cloned into pRSET (Invitrogen) for Set13 or pGEX6P-3 (GE Healthcare) or pTriEX-4 Hygro (Novagen) for Rpl42. To produce mutant Rpl42 proteins, the above plasmids were subjected to site-directed mutagenesis. Each expression vector was introduced into *E. coli* BL21 (DE3), and protein expression was induced by adding 1 mM isopropyl β-D-thiogalactopyranoside. The culture was incubated for 2 h more at 37 °C before harvesting, and the cells were then lysed by sonication (for His-Set13 and GST-Rpl42, -Rpl42-N, -Rpl42-M, and -Rpl42-C) or with buffer containing guanidine hydrochloride (for Rpl42-His and its derivatives). The expressed proteins were purified using TALON metal affinity resin (Clontech) or glutathione-Sepharose (GE Healthcare), according to the manufacturer's instructions. The eluted materials were dialyzed against phosphate-buffered saline or phosphate-buffered saline with 10% glycerol, divided into aliquots, and stored at −80 °C before use.

Antibodies—Anti-Rpl42 rabbit polyclonal antibodies were raised and affinity-purified using recombinant Rpl42-His. The purified antibodies were used for Western blot analyses. Other antibodies used in this study were anti-eIF2α [pS[52]] (Invitrogen, 44728G) and anti-tubulin (kindly provided by K. Gull).

In Vitro Methyltransferase Assay—*S. pombe* nuclear extracts of wild-type and Δ*set13* cells were prepared as described previously (39). The *in vitro* methyltransferase assay and the chromatographic fractionation of *S. pombe* nuclear extracts were performed as described previously (34).

Analysis of Methylated Peptide by Nano-liquid Chromatography-Tandem Mass Spectrometry (LC-MS/MS)—The LC-MS/MS analysis was performed as described previously (34).

Preparation of Ribosomes from HEK293T Cells—To prepare ribosomes from human cells, HEK293T cells were grown to ~80–90% confluence in 100-mm dishes, washed once with cold phosphate-buffered saline, and harvested using a rubber scraper. The cells were pelleted, resuspended in 2 volumes of homogenization buffer (10 mM Tris-HCl, pH 7.5, 5 mM MgCl$_2$, 10 mM KCl, 1 mM dithiothreitol), and lysed with a Dounce homogenizer. The lysate was freed of cell debris by centrifugation at 20,000 × g for 10 min at 4 °C. The supernatant was layered at a 1:1 ratio (v/v) over a sucrose cushion buffer (50 mM Tris-HCl, pH 7.5, 5 mM MgCl$_2$, 25 mM KCl, 2 M sucrose) and centrifuged at 100,000 × g for 24 h at 4 °C. The ribosome-enriched pellet was resuspended in homogenization buffer, and the proteins were resolved on 8–13% SDS-PAGE gels.

Microscopy Analysis—To analyze the localization of EGFP-fused Set13, wild-type *S. pombe* cells harboring the pREP1-EGFP-*set13* plasmid were grown to early log phase in liquid medium and washed twice with deionized H$_2$O, and the DNA was visualized by incubation with 1 μg/ml Hoechst 33342. To analyze the localization of green fluorescent protein-fused Rpl42, wild-type and Δ*set13* mutant *S. pombe* cells that had integrated the pDUAL-GFH1-*rpl42* construct were grown and treated as described above. Microscopic images were captured on a Zeiss

---

[3] The abbreviations used are: EGFP, enhanced green fluorescent protein; MTase, methyltransferase; LC-MS/MS, nano-liquid chromatography-tandem mass spectrometry; eIF2α, eukaryotic initiation factor 2α; AdoMet, *S*-adenosylmethionine.

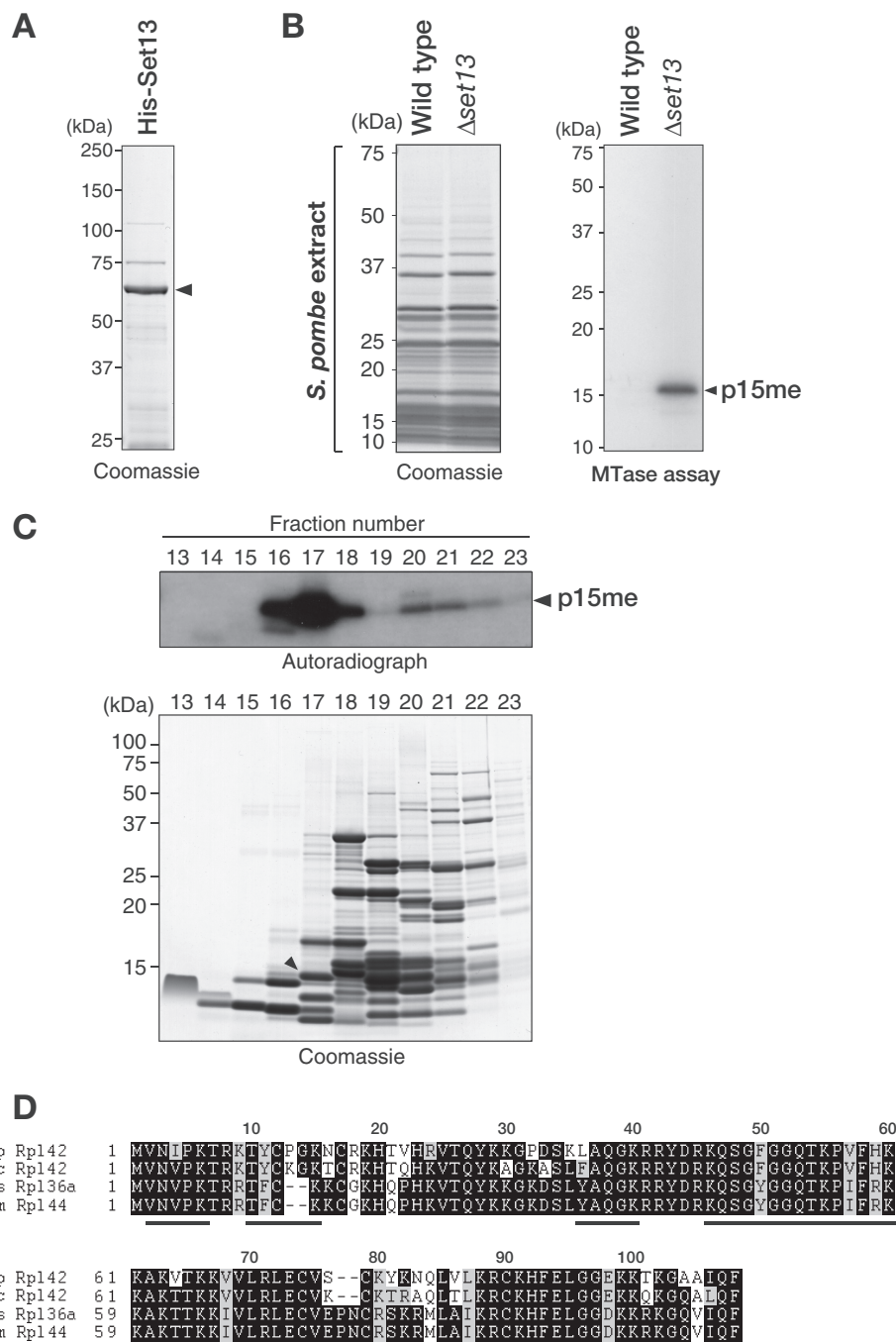# Rpl42 Methylation Regulates Ribosomal Function

FIGURE 1. **S. pombe Set13 specifically methylates a protein in nuclear lysates.** *A*, N-terminal His-tagged Set13 (*His-Set13*) was expressed in *E. coli* and purified by metal affinity chromatography. The eluted protein was resolved by 5–20% SDS-PAGE and visualized by Coomassie staining. His-Set13 is indicated by an *arrowhead*. *B, in vitro* MTase assay using *S. pombe* nuclear extracts. *S. pombe* nuclear extracts prepared from wild-type or Δ*set13* cells were resolved by 5–20% SDS-PAGE and visualized by Coomassie staining (*left*). These extracts were incubated with His-Set13 and [³H]AdoMet. The proteins were resolved by 15% SDS-PAGE, and labeled proteins were detected by autoradiography (*right*). The positions of size markers and labeled proteins are indicated, respectively, to the *left* and *right* of each image. *C,* fractionation of Set13 substrate(s) by reverse-phase chromatography. Nuclear extracts prepared from Δ*set13* cells were fractionated by reverse-phase chromatography. The proteins in each fraction were then concentrated and subjected to the *in vitro* MTase assay using His-Set13. After being resolved by 15% SDS-PAGE, the ³H-labeled proteins were detected by autoradiography (*top*), and the total proteins were detected by Coomassie staining (*bottom*). Protein(s) showing a similar migration profile to the ³H-labeled band is indicated by an *arrowhead*. *D,* amino acid sequences of *S. pombe* Rpl42 (*Sp Rpl42*), *S. cerevisiae* Rpl42 (*Sc Rpl42*), human Rpl36a (*Hs Rpl36a*), and *Mus musculus* Rpl44 (*Mm Rpl44*) aligned by the ClustalW 1.83 program. Identical amino acids are *heavily shaded*, and conserved amino acids are shown with *light shading*. The positions of peptide fragments identified in the LC-MS/MS analysis are indicated by *black lines* under the alignment.

Axioplan 2 imaging microscope and an ORCA-ER camera (Hamamatsu).

Spotting Assay—Wild-type and mutant cells were grown in YEA medium. 5-Fold serial dilutions were made from cultures of 1×10^7 cells/ml and spotted onto plates with YEA alone or YEA containing antibiotics of the indicated concentrations. To analyze the growth rate under different stress conditions, the spotted YEA plates were incubated at 30 °C for 2–4 days, 38 °C for 2–4 days, or 15 °C for 19 days.

Two-dimensional Electrophoretic Analysis of Proteins—The two-dimensional gel analysis of methylated proteins was performed as described previously (34).

Polysome Analysis—S. pombe cells were grown in 100 ml of YEA medium to mid-log phase (absorbance at 595 nm = 0.8) and harvested immediately following the addition of cycloheximide (100 μg/ml). The pelleted cells were washed with CH-cell-wash buffer (20 mM Tris-HCl, pH 7.5, 50 mM KCl, 10 mM MgCl$_2$, 1 mM dithiothreitol, 100 μg/ml cycloheximide, and 200 μg/ml heparin), suspended in 0.5 ml of CH-cell-lysis buffer (CH-cell-wash buffer supplemented with proteinase inhibitor mixture (Complete™ EDTA-free; Roche Applied Science)), and lysed with Multi-Beads Shocker (Yasui Kikai). An aliquot of the cleared lysate was overlaid on top of a 5–45% (w/v) sucrose gradient containing 20 mM Tris-HCl, pH 7.5, 50 mM KCl, 10 mM MgCl$_2$, 1 mM dithiothreitol, 100 μg/ml cycloheximide, 200 μg/ml heparin, and proteinase inhibitor mixture and centrifuged for 2 h at 36,000 rpm (222,000 × g_{max}) at 4 °C in a Beckman SW41TI rotor. The gradients were then fractionated using a Piston Gradient Fractionator (Biocomp). Polysome profiles were generated by continuous absorbance measurement at 254 nm using a UV monitor (Econo UV-monitor, Bio-Rad) connected to a chart recorder.

Quantitative Reverse Transcription-PCR Analysis of Cold-induced Genes—Yeast cells were grown until they reached $1–2 \times 10^7$ cells/ml,
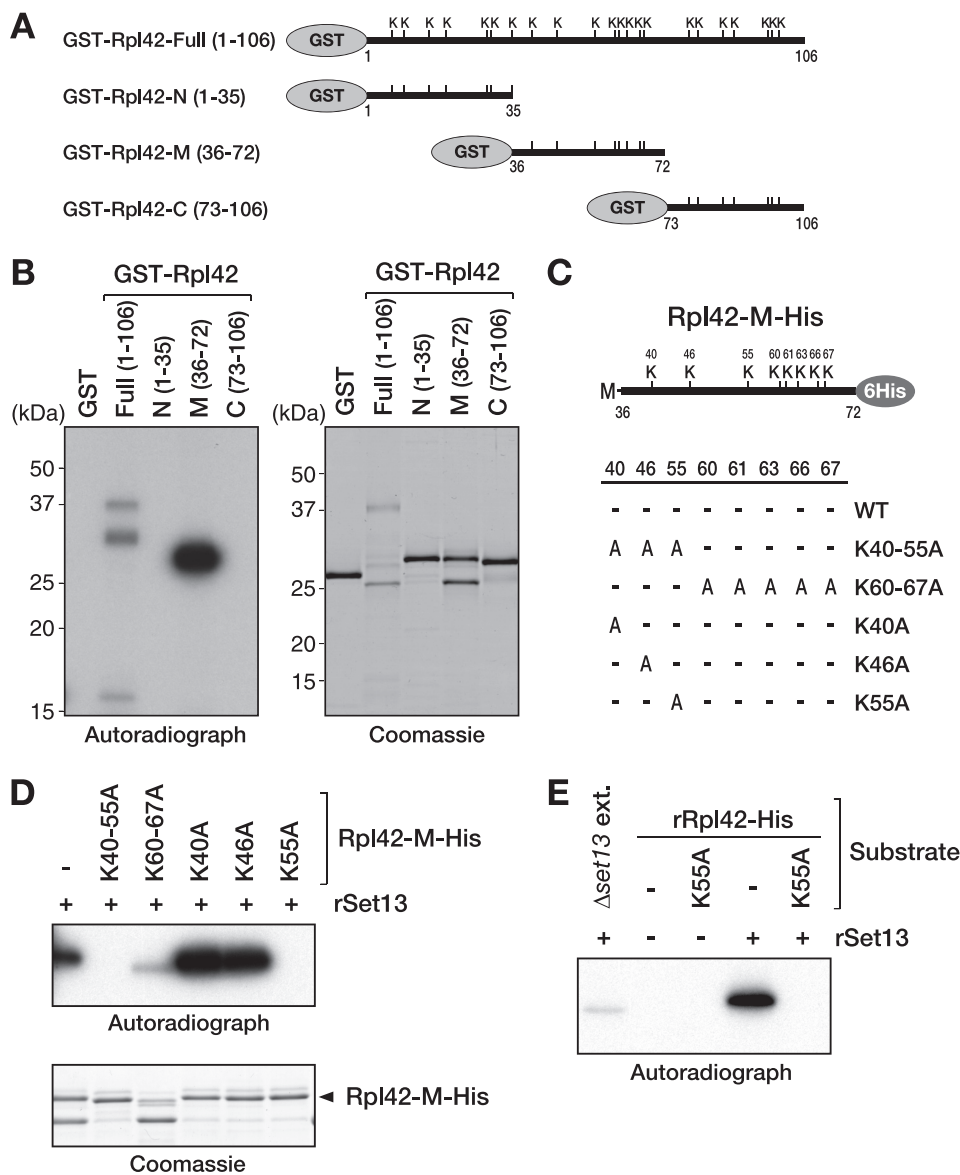
FIGURE 2. **Recombinant Rpl42 is methylated *in vitro* by His-Set13.** *A,* schematic drawing of full-length and three fragments of Rpl42 as follows: the N terminus (*GST-Rpl42-N*), the middle part (*GST-Rpl42-M*), and the C terminus of the protein (*GST-Rpl42-C*). The position of each lysine residue is indicated by a *K*. The amino acid numbers are also shown. *B, in vitro* MTase assay using recombinant Rpl42. GST-Rpl42-Full, GST-Rpl42-N, GST-Rpl42-M, and GST-Rpl42-C were incubated with His-Set13 and [³H]AdoMet. The proteins were resolved by 15% SDS-PAGE and visualized by Coomassie staining (*right*). Proteins methylated by Set13 were detected by autoradiography (*left*). *C,* schematic representation of the middle part of Rpl42 (*Rpl42-M-His*) and lysine candidates for methylation. These eight lysine residues were replaced by nonmethylatable alanine either alone or in combination. *A,* alanine; *WT,* wild type. *D* and *E, in vitro* MTase assay using recombinant alanine-substituted mutants of Rpl42. Alanine-substituted mutants of Rpl42-M-His (*D*) and Rpl42-His (*E*) were incubated with His-Set13 and [³H]AdoMet. The proteins were resolved by 15% SDS-PAGE and visualized by Coomassie staining (*D, bottom*). Proteins methylated by Set13 were detected by autoradiography (*D, top; E*).

$2\times$ one-step SYBR reverse transcription-PCR Buffer III, 0.4 μl of ROX reference dye, 0.8 μl of Prime-Script reverse transcription enzyme Mix II, 8 μM of each primer, 50 ng of template RNA, and RNase-free distilled H_2O to a total volume of 20 μl. The reverse transcription reaction (cDNA synthesis) was carried out at 42 °C for 5 min. The reaction mixture was then incubated at 95 °C for 10 s to inactivate the enzyme and denature the RNA/cDNA hybrid. The DNA amplification by PCR was next performed for 40 cycles, each cycle consisting of denaturation at 95 °C for 5 s, primer annealing, and extension at 60 °C for 31 s. The PCR product was subjected to dissociation conditions to confirm that it consisted of a single component. The relative mRNA amount was calculated and normalized to the amount of *act1*.

Survival in Stationary Phase—Yeast strains were streaked on YEA and grown for 5 days at 30 °C. From these plates, a preculture was inoculated on YEA and allowed to grow until it reached $1–2 \times 10^7$ cells/ml. This preculture was then used to inoculate a 100-ml culture. This culture was grown until the end of the exponential phase, when the A_{595} stopped increasing, and the cells had reached their maximum density. At this point, we started monitoring the cell survival by measuring the ability of individual yeast cells/organisms to form a colony (colony forming units). The cultures were serially diluted to reach a $1:2 \times 10^4$ dilution in YEA, and 100 μl of this dilution was plated in triplicate onto YEA plates. After 5–7 days, the total number of colonies was counted, with this number representing 100%
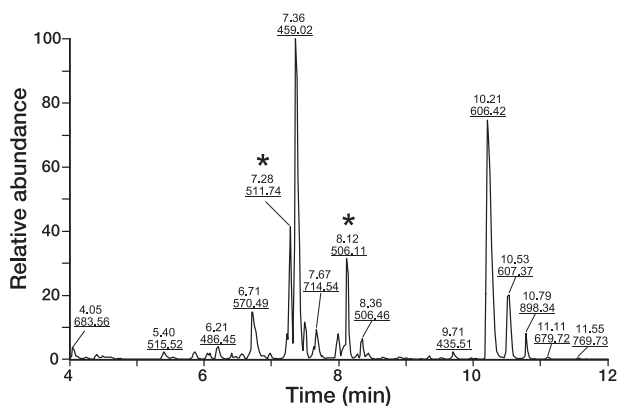
and then 15 ml of the yeast culture was collected for a time 0 reference. The cells were harvested by centrifugation, flash-frozen in liquid nitrogen, and stored at −80 °C until RNA preparation. The remaining cultured cells were cold-shocked at 15 °C in a precooled water bath and were further aerobically cultured at 15 °C. Cells were collected at 1, 4, 8, 24, and 30 h after the cold shock by centrifugation. The harvested cells were also flash-frozen and stored as described above. The total RNA was prepared by a hot phenol method (40). Real time PCR was performed using the Applied Biosystems 7300 real time PCR system. The following components were mixed on ice: 10 μl of

survival and day 0 of the curve. The subsequent measurements were taken every day.

RESULTS

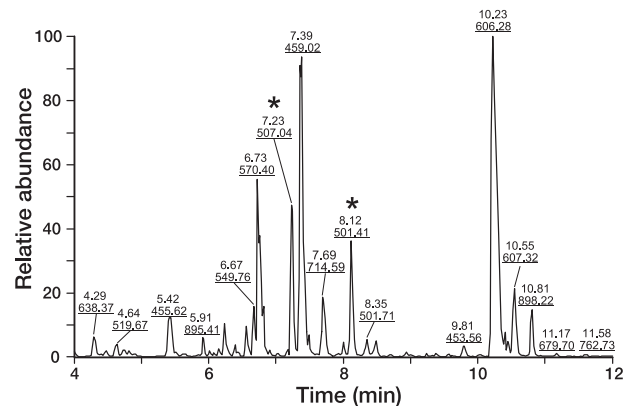*S. pombe Set13 Is an Active Methyltransferase That Modifies Ribosomal Protein L42*—Thirteen SET domain-containing proteins (SET proteins) have been identified in the *S. pombe* genome (supplemental Table S1). Using an *in vitro* methyltransferase (MTase) assay, we previously demonstrated that one of these SET proteins, Set11, specifically methylates ribosomal protein L11 (34). Here, we applied the same approach to
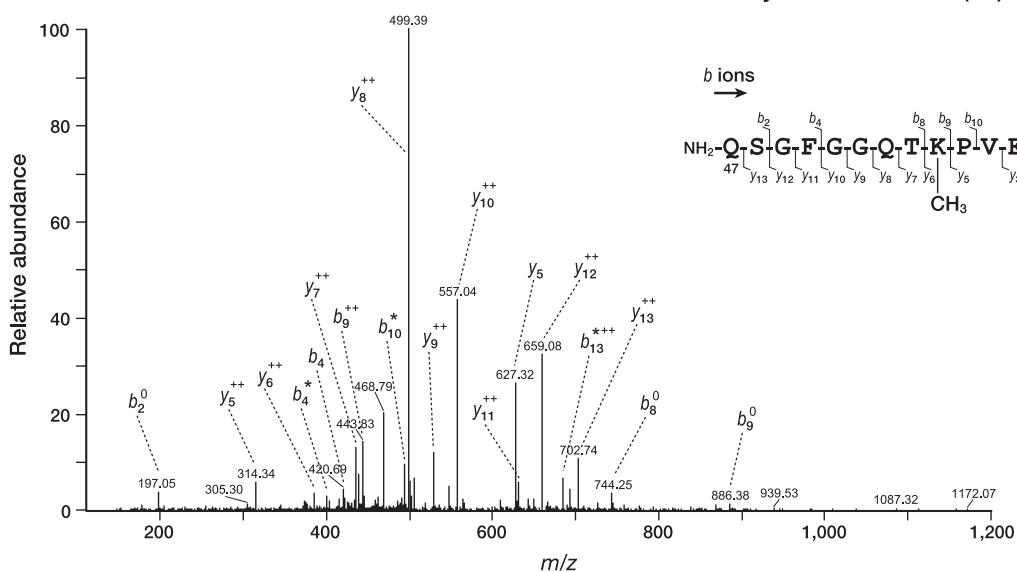
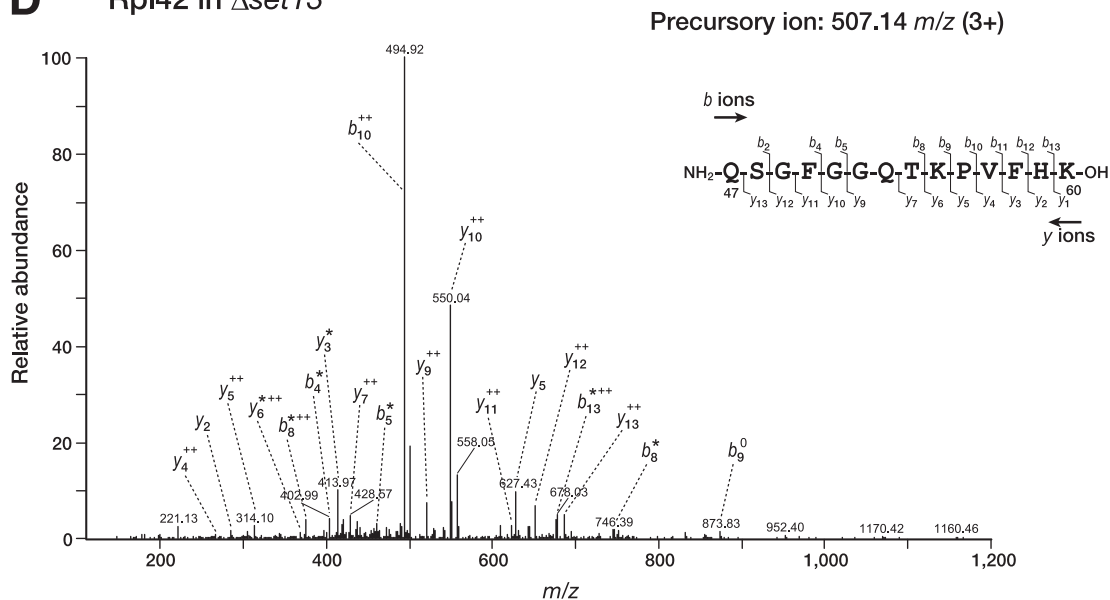# Rpl42 Methylation Regulates Ribosomal Function

A Rpl42 in wild-type

Relative abundance — Time (min)

4.05 683.56; 5.40 515.52; 6.21 486.45; 6.71 570.49; * 7.28 511.74; 7.36 459.02; 7.67 714.54; * 8.12 506.11; 8.36 506.46; 9.71 435.51; 10.21 606.42; 10.53 607.37; 10.79 898.34; 11.11 679.72; 11.55 769.73

B Rpl42 in Δset13

Relative abundance — Time (min)

4.29 638.37; 4.64 519.67; 5.42 455.62; 5.91 895.41; 6.67 549.76; 6.73 570.40; * 7.23 507.04; 7.39 459.02; 7.69 714.59; * 8.12 501.41; 8.35 501.71; 9.81 453.56; 10.23 606.28; 10.55 607.32; 10.81 898.22; 11.17 679.70; 11.58 762.73

C Rpl42 in wild type

Precursory ion: 511.37 m/z (3+)

Relative abundance — m/z

b ions →

NH$_2$-Q-S-G-F-G-G-Q-T-K-P-V-F-H-K-OH
47 ... 60
CH$_3$
y ions ←

b_2, b_4, b_8, b_9, b_{10}, b_{13}
y_{13}, y_{12}, y_{11}, y_{10}, y_9, y_8, y_7, y_6, y_5, y_3

Labeled peaks: b_2^0 197.05; y_5^{++} 305.30; 314.34; y_6^{++}; b_4^*; b_4; b_9^{++}; b_{10}^*; 420.69; 443.83; 468.79; y_7^{++}; 499.39; y_8^{++}; y_9^{++}; 557.04; y_{11}^{++}; 627.32; y_5; 659.08; y_{12}^{++}; b_{13}^{*+++}; 702.74; y_{13}^{++}; 744.25; b_8^0; b_9^0 886.38; 939.53; 1087.32; 1172.07

D Rpl42 in Δset13

Precursory ion: 507.14 m/z (3+)

Relative abundance — m/z

b ions →

NH$_2$-Q-S-G-F-G-G-Q-T-K-P-V-F-H-K-OH
47 ... 60
y ions ←

b_2, b_4, b_5, b_8, b_9, b_{10}, b_{11}, b_{12}, b_{13}
y_{13}, y_{12}, y_{11}, y_{10}, y_9, y_7, y_6, y_5, y_4, y_3, y_2, y_1

Labeled peaks: 221.13; y_4^{++}; 314.10; y_5^{++}; y_2; y_6^{*+++}; b_8^{*+++}; 402.99; b_4^*; 413.97; y_3^*; 428.57; y_7^{++}; b_5^*; 494.92; b_{10}^{++}; y_9^{++}; 550.04; y_{10}^{++}; 558.05; y_{11}^{++}; 627.43; y_5; 678.93; y_{12}^{++}; b_{13}^{*+++}; 746.39; y_{13}^{++}; b_8^*; b_9^0 873.83; 952.40; 1170.42; 1160.46

investigate the cellular function of Set13, a previously uncharacterized SET protein encoded by *SPAC688.14*.

We prepared a recombinant His-tagged full-length Set13 (His-Set13) (Fig. 1*A*) and incubated it with acid-extracted nuclear extracts prepared from wild-type or Δ*set13 S. pombe* cells in the presence of ³H-labeled methyl donor ([³H]AdoMet). Although specific methylation signals were not detected in the assay using an extract from wild-type cells, a strongly methylated band with a molecular mass of ~15 kDa on SDS-PAGE was detected in the assay using the Δ*set13* cell extract (Fig. 1*B*, *p15me*). This result suggested that Set13 is an active methyltransferase and that p15 is one of the physiological targets of Set13. As was the case for Set11 (34), the methylation site(s) may have been modified already by endogenous Set13 in the wild-type cells.

To identify the target protein(s) of Set13, we separated the nuclear extracts of Δ*set13* mutant cells by reverse-phase chromatography, and the eluted proteins were tested in the *in vitro* MTase assay. As shown in Fig. 1*C*, the target protein(s) was eluted in several fractions, with a peak at fraction 17. The protein band showing the same elution profile in the chromatography (Fig. 1*C*, indicated by an *arrowhead*) was excised from the gel and subjected to LC-MS/MS analysis. In parallel with this chromatographic approach, we separated the methylated product(s) by two-dimensional acetic acid/urea/Triton X-100 (AUT) and acetic acid/urea/acetyltrimethylammonium bromide (AUC) gel analysis (34). After two-dimensional separation, one discrete signal was detected in the autoradiograph (supplemental Fig. S1). The protein spot corresponding to this signal was excised and subjected to LC-MS/MS analysis. From both the chromatographic (Fig. 1*C*) and two-dimensional gel (supplemental Fig. S1) approaches, we obtained a series of peptides that matched perfectly with the deduced amino acid sequence of the *S. pombe* ribosomal large subunit protein L42 (Rpl42) (Fig. 1*D*, indicated by *underlines*). Rpl42 is highly conserved from yeast to humans (Fig. 1*D*), and its structural homologue was also identified in *Haloarcula* (41).

Set13 Modifies Recombinant Rpl42 in Vitro—To confirm that Rpl42 is a physiological substrate for Set13, an *in vitro* MTase assay was performed using recombinant full-length Rpl42 (GST-Rpl42-Full) (Fig. 2*A*). The full-length GST-Rpl42 was clearly methylated by Set13 (Fig. 2*B*), indicating that Rpl42 is indeed a substrate for Set13. To determine the methylation site(s) on Rpl42, we separated Rpl42 into the following three parts: N terminus (*N*); middle (*M*) part; and C terminus (*C*), and the GST fusion proteins containing each part (Fig. 2*A*) were used in the MTase assay. Set13 selectively methylated the GST fusion protein containing the middle part of Rpl42 (Fig. 2*B*, *GST-Rpl42-M*), suggesting that the methylated residue(s) resides in amino acids 36–72 of Rpl42.

To identify the site of Rpl42 methylation, we introduced a series of alanine substitutions for the candidate lysine residues

in Rpl42-M-His, either alone or in combination (Fig. 2*C*), and we used these mutant proteins in the *in vitro* MTase assay. Although the K60–67A mutation decreased the Set13 activity, the K40–55A mutation completely abolished it (Fig. 2*D*, *Rpl42-M-His^{K40−55A}*). Further detailed mapping revealed that the single alanine substitution of lysine 55 (K55A) clearly blocked the Set13 MTase activity (Fig. 2*D*, *Rpl42-M-His^{K55A}*). We also confirmed that the same K55A mutation in full-length Rpl42 (rRpl42-His) abolished the Set13 activity (Fig. 2*E*). Together, these results indicate that Rpl42 is a physiological substrate of Set13 and that lysine 55 of Rpl42 is the candidate target residue for Set13. The reduced activity seen with the K60–67A mutant (Fig. 2*D*) may have been caused by poor substrate recognition by Set13, because these mutations could have altered the local structure of the protein.

Determination of the Methylation Sites of Rpl42 by LC-MS/MS—To determine the *in vivo* methylation site of Rpl42, the endogenous Rpl42 in wild-type or Δ*set13* cells was isolated by reverse-phase chromatography (as shown in Fig. 1*C*) and analyzed using LC-MS/MS. Although the overall elution profiles of the digested Rpl42 peptides in the nano-LC spectra were superimposable, the representative masses of several eluted peptides were different between the wild-type and Δ*set13* cells (Fig. 3, *A* and *B*, indicated by *asterisks*). The experimental mass of the faster eluted peptides obtained from a linear ion trap time-of-flight system was 1532.04 (MH⁺) for wild-type cells and 1517.99 (MH⁺) for Δ*set13* cells (supplemental Table S2, NanoFrontierLD), and the mass difference was 14.05 Da, which corresponds to the mass of one methyl group. A similar mass difference was observed for a slower eluted fragment at 8.12 min.

MS/MS analysis revealed that the amino acid sequence of both the faster and slower eluted fragments matched the 47–60 residues of Rpl42 and that the slower eluted peptide was a deaminated derivative of the faster eluted peptide (Fig. 3, *C* and *D*, and supplemental Table 2). Importantly, the peptide in wild-type cells was monomethylated at lysine 55 (Fig. 3*C*), whereas the corresponding residue in Δ*set13* cells was unmodified (Fig. 3*D*). This result is consistent with our *in vitro* MTase assay results (Fig. 2*E*) and suggests that Set13 is a specific MTase that monomethylates lysine 55 of Rpl42.
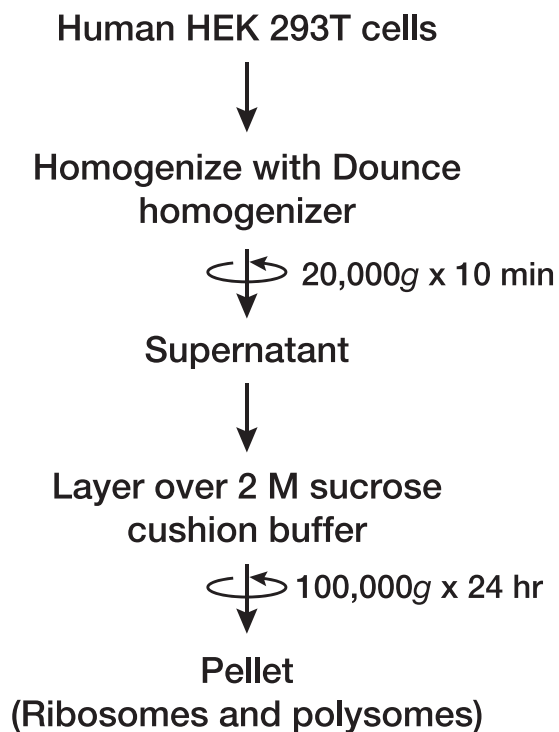
By analyzing the MS/MS results, we were able to identify additional methylated peptides from the Rpl42 of wild-type cells (supplemental Table S3). We found, however, that these modifications were present in the Δ*set13* cells and that the corresponding unmethylated peptides were frequently detected in both wild-type and Δ*set13* cells. Thus, it is unlikely that these additional lysine residues are the physiological targets of Set13.

Rpl42 Methylation at Lysine 55 Is Conserved from Yeast to Humans—Rpl42 is evolutionarily conserved among eukaryotes, and the methylation at lysine 55 has also been identified in other species, including budding yeast (16) and plants
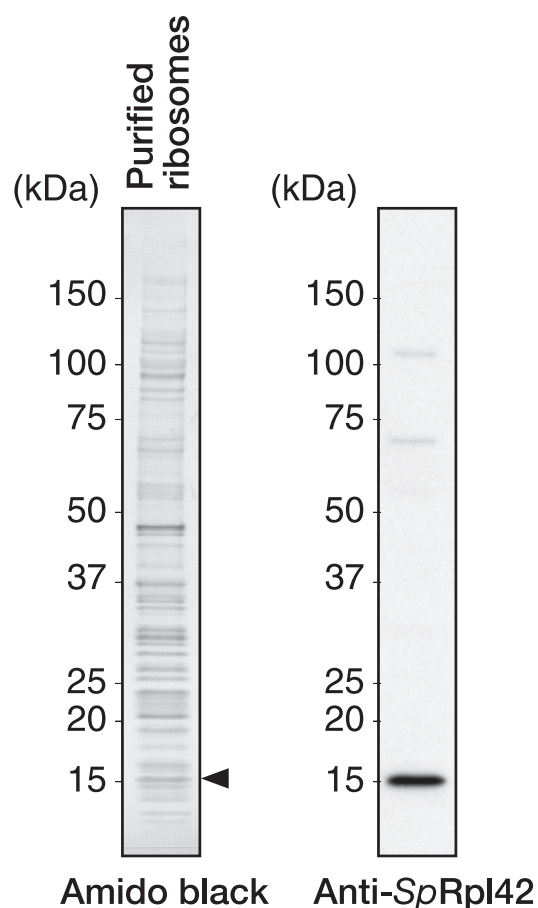
FIGURE 3. **LC-MS/MS analysis of Rpl42 derived from wild-type and Δ*set13 S. pombe*.** Rpl42 was isolated from wild-type or Δ*set13* mutant cells by reverse-phase chromatography, digested with trypsin, and analyzed using a quadrupole ion trap mass spectrometer (Finnigan LTQ; Thermo Fisher Scientific). *A* and *B*, base peak, ion chromatogram for a 12-min separation of the digested Rpl42 peptides from the wild-type (*A*) and Δ*set13* strains (*B*). The elution time (*upper*) and representative *m/z* (*lower, underlined*) of the eluted peptides are indicated at the top of each peak. The peaks for the peptide fragment spanning residues 47–60 are indicated by an *asterisk*. *C* and *D*, MS/MS spectra of the peptide fragment spanning residues 47–60 from the wild-type (*C*) and Δ*set13* strains (*D*) are shown. The observed *y* and *b* ions and fragment map are shown.
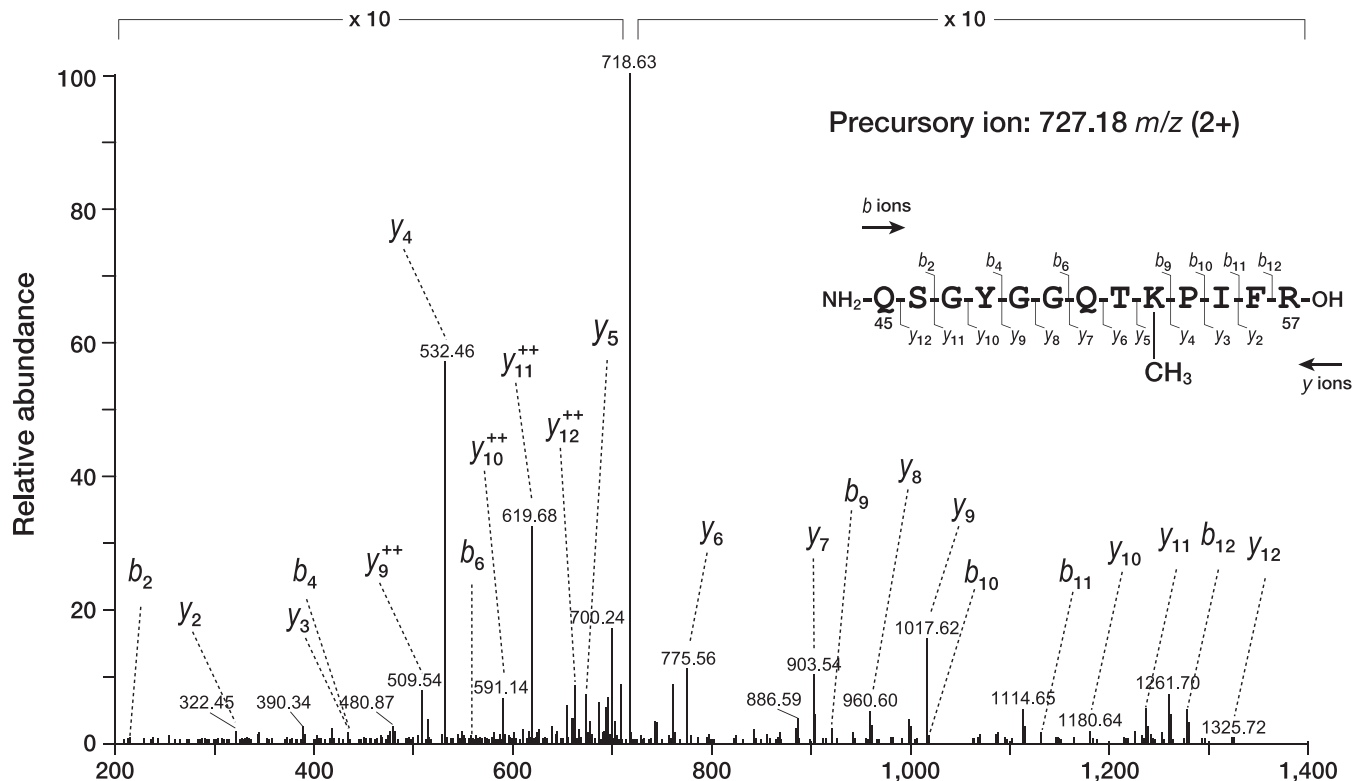
Rpl42 Methylation Regulates Ribosomal Function

A

Human HEK 293T cells

↓

Homogenize with Dounce
homogenizer

↻ 20,000*g* x 10 min

Supernatant

↓

Layer over 2 M sucrose
cushion buffer

↻ 100,000*g* x 24 hr

Pellet
(Ribosomes and polysomes)

B

(kDa) Purified ribosomes

150
100
75
50
37
25
20
15 ◄

Amido black

(kDa)

150
100
75
50
37
25
20
15

Anti-*Sp*Rpl42

C Rpl36a in human 293T cells

Precursory ion: 727.18 *m/z* (2+)

b ions →

NH₂-Q-S-G-Y-G-G-Q-T-K-P-I-F-R-OH
45   57

CH₃

← *y* ions

(19). To obtain further evidence for the importance of the Rpl42 methylation, we determined whether the methyl modification is present on human Rpl36a, the homologue of *S. pombe* Rpl42 (Fig. 1*D*).

Ribosomes were purified from HEK293T cell extracts by centrifugation, and the associated proteins were resolved by SDS-PAGE (Fig. 4, *A* and *B*). Human Rpl36a, detected by an anti-*Sp*Rpl42 antibody (Fig. 4*B*, indicated by an *arrowhead*), was excised and subjected to the LC-MS/MS analysis. Mass spectrometric analysis revealed that human Rpl36a was also monomethylated at lysine 53, which corresponds to lysine 55 of *S. pombe* Rpl42 (Fig. 4*C*). The high conservation of Rpl42 methylation suggests that it has an important role in the ribosomal function.

Location of Rpl42 and Lysine 55 on the Large Ribosomal Subunit—To gain insight into the role of Rpl42 methylation, we examined the structure and relative position of Rpl42 on the large ribosomal subunit. Because structural information on the *S. pombe* ribosome is not yet available, we used the previously characterized cryo-EM structure of the *S. cerevisiae* 80 S ribosome (42) to visualize the three-dimensional structure and relative location of Rpl42 in the large ribosomal subunit (Fig. 5, *A* and *B*). Rpl42 has a large loop extension and is positioned between the central and L1 protuberances of the large ribosomal subunit. Within Rpl42, lysine 55 is located in this loop extension and lies close to the E-site (Fig. 5, *A* and *B*, indicated by *yellow*).

In *Haloarcula marismortui*, the L44e protein, the structural homologue of Rpl42, is located at the same position in the large ribosomal subunit (41) and interacts through its loop extension with an RNA oligonucleotide that mimics the CCA end of deacylated tRNA bound to the E-site (43). Lysine 51, one of the L44e residues that make specific contact with the cytosine 75 of CCA (Fig. 5*C*, indicated by *pink arrowheads*), corresponds to lysine 55 of Rpl42. Thus, Rpl42 methylation may play a role in the recognition of deacylated tRNA bound to the E-site, although this possibility needs to be clarified by further detailed structural analyses.

Set13 Predominantly Localizes to the Nucleus—To gain further insight into the function of the Set13 methyltransferase, we examined its localization by expressing it as an EGFP fusion protein. EGFP-Set13 predominantly localized to the nucleus, including both the nucleolus and the other 4′,6-diamidino-2-phenylindole-dense nuclear hemisphere (Fig. 5*D*) (37), suggesting that Set13 modifies Rpl42 in the nucleus, presumably prior to ribosome assembly. Because the localization of Rpl42-GFP was the same for wild-type and Δ*set13* cells (Fig. 5*E*), it is likely that the assembly of Rpl42 into the ribosome is independent of its methylation.

Rpl42 Methylation-defective Mutants Show Cycloheximide Sensitivity—Cycloheximide is a potent protein synthesis inhibitor that blocks translational elongation by interfering with the

peptidyltransferase activity of the 60 S ribosome. In several organisms, mutations in the large ribosomal subunit lead to a recessive cycloheximide-resistant phenotype (44). One of these mutations maps to proline 56 of Rpl42 (45), which is close to lysine 55 (Fig. 5*A*, indicated in *blue*). This result prompted us to investigate the role of Set13 and Rpl42 methylation in cycloheximide sensitivity.

The Δ*set13* mutant cells were viable and showed no noticeable growth defects under normal culture conditions (*e.g.* see Fig. 6*B*, *0 μg/ml CYH*). However, the Δ*set13* cells displayed higher cycloheximide sensitivity than wild-type cells (Fig. 6*B*, *10* and *20 μg/ml CYH*). The increased sensitivity was not attributable to a change in the Rpl42 protein level, which was comparable between wild-type and Δ*set13* cells (Fig. 6*A*). To rule out the possibility that other Set13 substrates indirectly affected the cycloheximide sensitivity, we introduced two amino acid substitutions (K55R and P56Q) into the *rpl42*[+] gene, and we examined the cycloheximide sensitivity. As observed previously (45), the *rpl42*[P56Q] mutation conferred a strong resistance to cycloheximide (Fig. 6, *A* and *B*). In contrast, the *rpl42*[K55R] mutant cells were even more sensitive to cycloheximide than the Δ*set13* cells, although the Rpl42 protein level was the same (Fig. 6, *A* and *B*). Taken together, these results demonstrated that Set13 and Rpl42 methylation play a direct role in cycloheximide sensitivity, which is tightly linked to ribosomal function. The greater sensitivity of *rpl42*[K55R] cells to cycloheximide was presumably due to the imperfect mimicry of the lysine residue by arginine.

To gain further insight into the roles of Set13 and the methylation of Rpl42 in ribosomal function, we examined whether the Δ*set13* and *rpl42* mutant cells were sensitive to other ribosome-targeting translational inhibitors, including anisomycin, paromomycin, G418, and hygromycin (46–48). Intriguingly, the Δ*set13* and *rpl42* mutant cells showed no clear sensitivity to these translational inhibitors, and only the *rpl42*[K55R] cells showed a weak resistance to hygromycin (supplemental Fig. S2). These results suggested that methylated Rpl42 contributes to particular step(s) in the peptidyltransferase reaction rather than affecting overall ribosomal function. Considering its location and a previous observation that cycloheximide arrests the ribosome when the first deacylated tRNA reaches the E-site (49), it is likely that cycloheximide blocks elongation by interacting with the E-site when it contains deacylated tRNA, and that Rpl42 methylation-defective mutant cells affect the binding or affinity of cycloheximide.

Rpl42 Methylation-defective Mutants Show Abnormal Cell Growth under Various Environmental Stresses—We next examined whether Set13 and Rpl42 methylation are involved in other cellular processes that are linked to ribosomal function. As described above, Rpl42 methylation-defective mutant cells showed no obvious growth defects under normal culture conditions (Fig. 6*B*). This finding was confirmed by a polysome

FIGURE 4. **Human Rpl36a is methylated at lysine 53 *in vivo*.** *A,* procedure for preparing ribosomes and polysomes from HEK293T cells. *B,* detection of human Rpl36a using an anti-*Sp*Rpl42 antibody. Proteins were resolved by 8–16% SDS-PAGE and visualized by Coomassie staining (*left*). Rpl36a detected by the anti-*Sp*Rpl42 antibody is shown (*right*). The protein showing a similar migration as the Western blot signal is indicated by an *arrowhead*. *C,* LC-MS/MS analysis of human Rpl36a. Rpl36a excised from an SDS-polyacrylamide gel was digested with trypsin, and the digested peptides were subjected to LC-MS/MS analysis. The MS/MS spectrum of the peptide fragment spanning residues 45–57 is shown. The observed *y* and *b* ions and fragment map are shown.
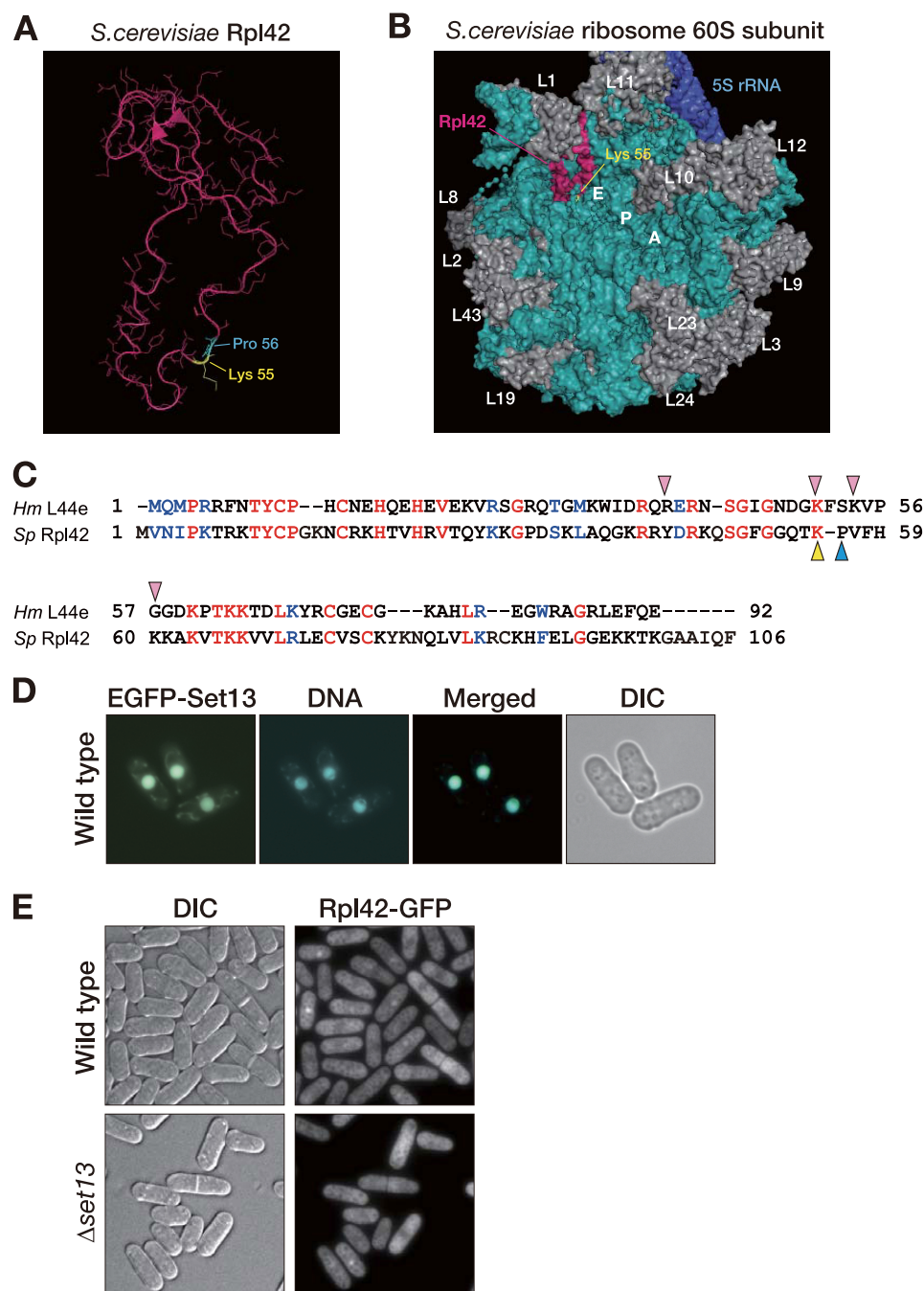
Rpl42 Methylation Regulates Ribosomal Function

FIGURE 5. **Overview of Rpl42 on the large subunit of the ribosome.** *A,* structure of *S. cerevisiae* Rpl42 (42). *Blue,* proline 56 of Rpl42; *yellow,* lysine 55 of Rpl42. *B,* surface view of the large subunit of the *S. cerevisiae* ribosome (Protein Data Bank file 1S1I) (42). *Pink,* Rpl42; *aqua,* 5.8 S/25 S ribosomal RNA; *blue,* 5 S ribosomal RNA; *yellow,* lysine 55 of Rpl42. The locations of the E-site, P-site, and A-site are indicated. The visible proteins are identified. *C,* amino acid sequences of *S. pombe* Rpl42 and *H. marismortui* L44e aligned by the ClustalW 2 program. Identical amino acids are in *red,* and conserved amino acids are in *blue. Pink arrowheads* indicate the main residues that interact with the 3′-CCA end of tRNA. *Yellow arrowhead* indicates the residue that is methylated in *S. pombe* Rpl42. *Blue arrowhead* indicates the residue whose substitution confers resistance to cycloheximide. *D,* EGFP-fused Set13 predominantly localized to the nucleus. EGFP-fused Set13 was expressed from the *nmt1* promoter in wild-type cells. The cells were stained with Hoechst 33342 (DNA). A merged image of the EGFP-Set11 and DNA (*Merged*), and differential interference contrast (*DIC*) image are also shown. *E,* green fluorescent protein-fused Rpl42 mainly localized to the cytoplasm and the nucleolus. Rpl42-GFP was expressed from the *nmt1* promoter in wild-type or Δ*set13* cells. The differential interference contrast image is also shown.

type cells. We noticed, however, that unlike the wild-type cells, the Δ*set13* and the *rpl42^{K55R}* mutant cells showed robust growth at low temperature (Fig. 6C, *15 °C*). In addition, these mutant cells showed resistance, to different degrees, to other stress conditions such as high temperature (Fig. 6C, *38 °C*), high salt concentration (Fig. 6D), and glucose starvation (Fig. 6E). The *rpl42^{K55R}* cells showed stronger effects compared with the Δ*set13* cells. The cycloheximide-resistant *rpl42^{P56Q}* mutant cells also displayed abnormal responses to these environmental stresses. Interestingly, the *rpl42^{P56Q}* mutant cells showed the opposite phenotype for high temperature (Fig. 6C, *38 °C*) and glucose starvation (Fig. 6E) to that observed for the Δ*set13* and *rpl42^{K55R}* cells. Together, these results demonstrated that Set13 and Rpl42 methylation are required for proper growth control under various stress conditions and suggest that the E-site configuration determined by Rpl42 may control ribosomal function under these environmental stresses.

Cold Adaptation of Rpl42 Methylation-defective Mutants Is Independent of the General Stress-response Pathways—Among several stress conditions that we examined, the Rpl42 methylation-defective mutant cells displayed the greatest differences under the low temperature condition (15 °C) (Fig. 6C). Although this temperature is far below that of laboratory culture conditions (~30 °C), it commonly occurs in the natural world; therefore, the phenotype appears to be linked with important cell survival responses. To investigate the role of Rpl42 methylation further, we focused on this cold-adaptive phenotype.

Cells first grown at 30 °C were shifted to 15 °C, and the cellular growth after the temperature shift was monitored (Fig. 7A). Upon the shift to the low temperature (Fig. 7A, *0 h*), the growth rate of the wild-type cells immediately slowed, although they continued to grow. Although the Δ*set13* and *rpl42* mutant cells showed a similar growth arrest

analysis that showed similar levels of 40 S, 60 S, and 80 S ribosomes and comparable profiles of polyribosomal components (supplemental Fig. 3) in the methylation-defective and wild-
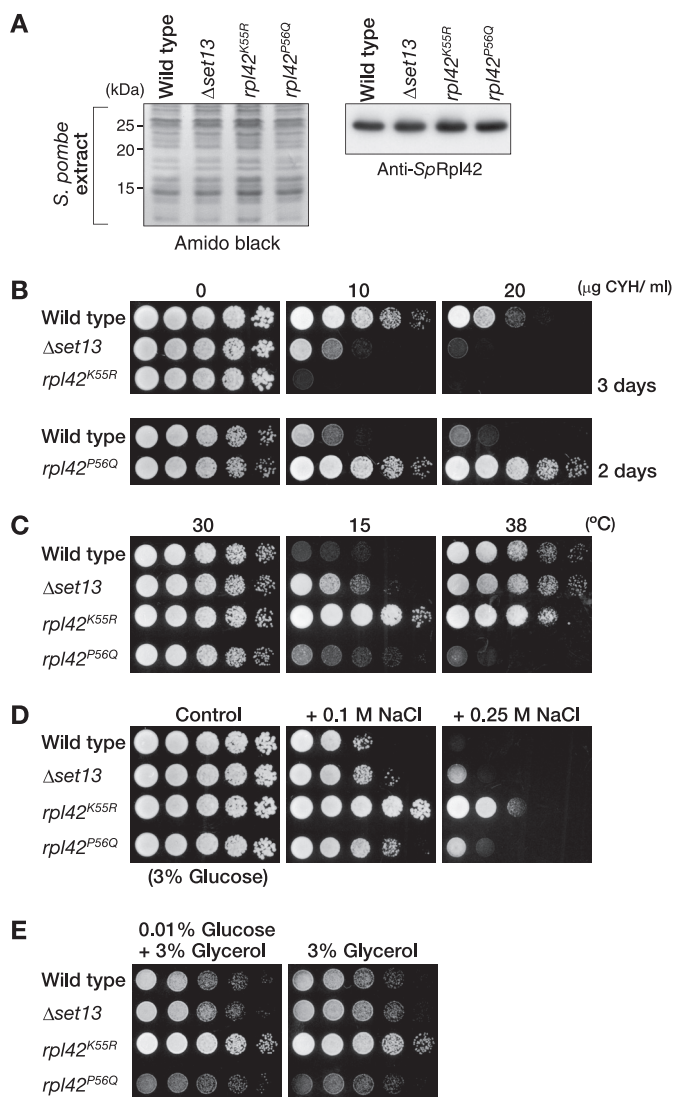
FIGURE 6. **Rpl42 methylation-defective mutants show abnormal cell growth under environmental stresses.** *A*, protein levels of Rpl42 in the $\Delta set13$, $rpl42^{K55R}$, and $rpl42^{P56Q}$ mutant cells. Exponentially growing cultures of wild-type, $\Delta set13$, $rpl42^{K55R}$, and $rpl42^{P56Q}$ cells in YEA were harvested. The total cell lysates prepared from these strains were resolved on a 12.5% SDS-polyacrylamide gel. Rpl42 was detected by Western blotting with an anti-SpRpl42 antibody (*right*). As a loading control, the Amido Black stained blot is shown (*left*). *B*, $\Delta set13$ and the $rpl42^{K55R}$ mutant cells showed a greater sensitivity to cycloheximide. 5-Fold dilutions of wild-type, $\Delta set13$, and $rpl42^{K55R}$ cells were plated onto YEA alone or YEA containing different doses of cycloheximide for 3 days (*top*). 5-Fold dilutions of wild-type and $rpl42^{P56Q}$ mutant cells were plated onto YEA alone or YEA containing different doses of cycloheximide for 2 days (*bottom*). *C*, set13-null and $rpl42^{K55R}$ mutant cells showed resistance against cold stress. 5-Fold dilutions of wild-type, $\Delta set13$, $rpl42^{K55R}$, and $rpl42^{P56Q}$ cells were plated onto YEA at 30, 38, or 15 °C for 2, 3, or 19 days, respectively. *D* and *E*, $rpl42^{K55R}$ mutant cells showed resistance against environmental stresses. 5-Fold dilutions of each strain were plated onto YEA alone, YEA containing different doses of NaCl (*D*), YEA containing 3% glycerol instead of glucose, or YEA containing 0.01% glucose plus 3% glycerol (*E*), for 3 days.

at the time of the temperature shift, their growth, following adaptation, was clearly different from that of wild-type cells (Fig. 7*A*), *i.e.* the $\Delta set13$ and $rpl42$ mutant cells showed a normal response to the temperature shift but grew at an abnormal rate under cold-adapted conditions. The expression profiles of known cold-induced genes (supplemental Fig. S4) supported the notion that the initial cold responses functioned properly in these mutant cells.

The $rpl42^{K55R}$ mutant cells showed a higher growth rate than the wild-type cells, consistent with the spotting assay (Fig. 6*C*). In contrast, the $\Delta set13$ and $rpl42^{P56Q}$ mutant cells showed a lower growth rate (Fig. 7*A*). For $\Delta set13$, this was seemingly in contrast to the results of the spotting assay (Fig. 6*C*). We think, however, that these mutants may simply have needed a longer time to recover from the cold-induced growth arrest, because once they recovered, their cold-adapted growth was faster than that of wild-type cells.

Translational control is tightly linked to stress responses. Many different types of stress reduce global translation by triggering the phosphorylation of eIF2α, which is mediated by stress-activated protein kinases, Gcn2 and Hri2, in fission yeast (50). To investigate the relationship between Rpl42 methylation and the global stress-response pathway, we combined $\Delta gcn2$ with the $\Delta set13$ or $rpl42$ mutations and examined the growth of these double mutant cells under stress conditions (Fig. 7*B*). Although the $\Delta gcn2$ mutation itself caused a weak growth defect or resistance under the stress conditions, it caused little or no change in the cold-adapted growth of $\Delta set13$ or $rpl42$ mutant cells. The same was true for $\Delta hri2$ mutant cells (data not shown). In addition, cold stress did not trigger the phosphorylation of eIF2α (Fig. 7*C*), whereas heat-shock stress did induce the phosphorylation. These results suggested that the cold-adapted growth of Rpl42 methylation-deficient cells was not coupled to the eIF2α-mediated stress-response pathway.

We also explored potential genetic links between the $\Delta set13$ mutation and other stress-response pathways such as the target of rapamycin (51) and the stress-activated protein kinase (52). However, we did not find any correlations with the cold-adapted growth of Rpl42 methylation-deficient cells (data not shown). Therefore, it is likely that the cold-adapted growth of $\Delta set13$ and $rpl42^{K55R}$ mutant cells was caused, at least in part, by an altered physical property of ribosomes rather than by defects in the stress-response pathways.

Rpl42 Methylation Is Linked to Chronological Aging—The $\Delta set13$ and $rpl42^{K55R}$ mutant cells appeared to have a growth advantage under several stress conditions, although the global stress-response pathway was maintained. However, it is possible that proper growth suppression under such stress conditions is beneficial to the survival of the population. Consistent with this idea, we frequently observed that these mutant cells recovered poorly after prolonged storage in the laboratory refrigerator (data not shown). Thus, to determine the potential involvement of Rpl42 methylation in population survival, we examined cell viability after the cells entered the stationary phase.

The viability of individual yeast cells decreases with the time they spend in stationary phase, a phenomenon known as chronological aging (53, 54). To study the role of Rpl42 methylation in this process, the $\Delta set13$ and $rpl42$ mutant cells were grown until the stationary phase, and their survival rate was determined by counting the colony-forming units. Under our experimental conditions using rich culture medium, 99.9% of the wild-type cells died after 9 days (Fig. 8*A*). Interestingly, the $\Delta set13$ and $rpl42^{K55R}$ mutant cells exhibited roughly half the life span of wild-type cells, with the $rpl42^{K55R}$ mutant cells

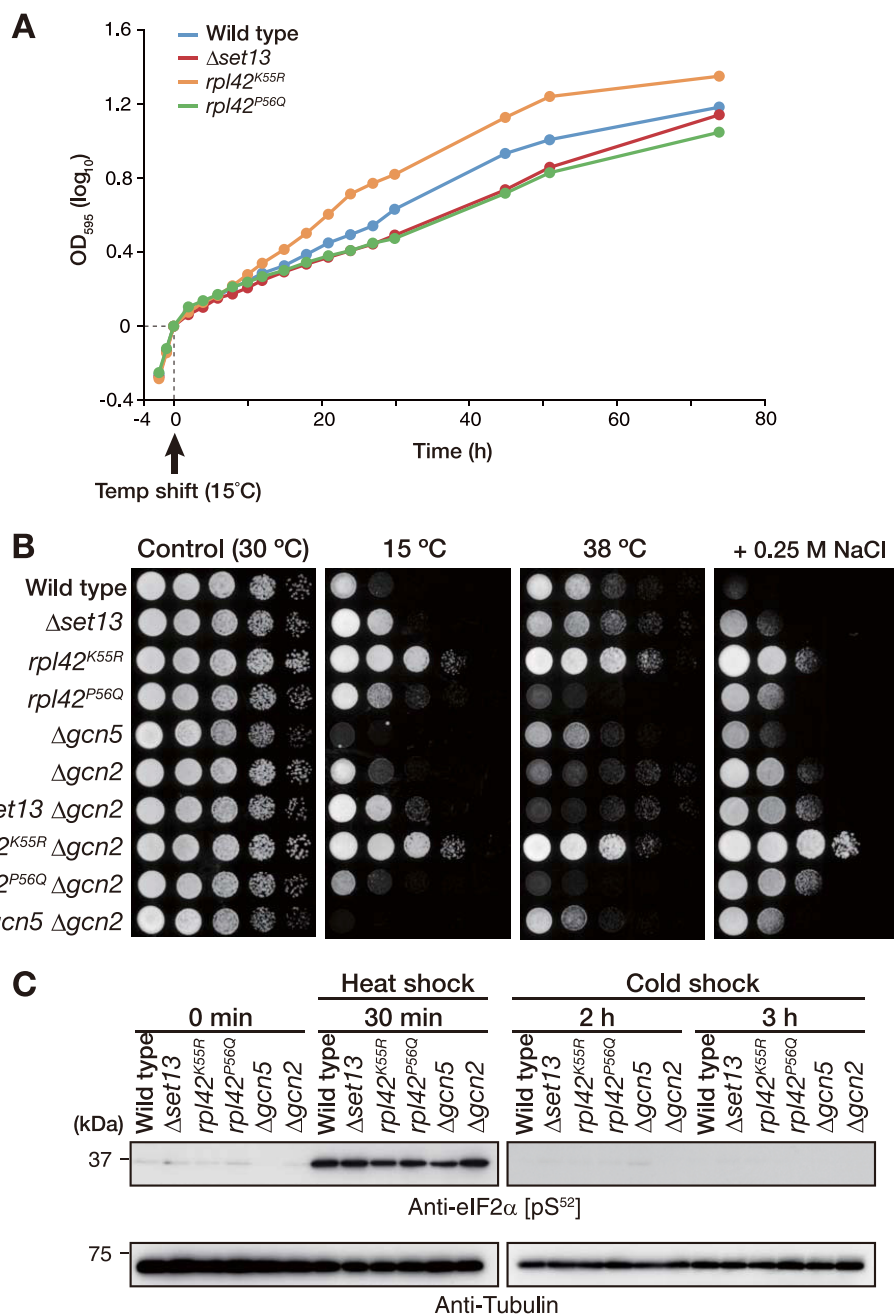# Rpl42 Methylation Regulates Ribosomal Function

FIGURE 7. **Cold-adapted growth of Rpl42 methylation-defective mutants is independent of general stress-response pathways.** *A,* effect of cold shock on cell growth. Wild-type (*blue*), $\Delta set13$ (*red*), $rpl42^{K55R}$ (*orange*), and $rpl42^{P56Q}$ (*green*) cells were grown until the mid-log phase in YEA medium at 30 °C. The cells were then shifted to 15 °C at time 0. Cell growth was monitored by measuring A_{595} (OD_{595}). *B,* no genetic interaction between *gcn2* and methylation-defective mutants was observed. 5-Fold dilutions of each strain were plated onto YEA containing 0.25 M NaCl for 4 days or YEA alone at 30, 38, or 15 °C for 2, 3, or 19 days, respectively. *C,* methylation-deficient mutation did not affect eIF2α phosphorylation in response to cold stress or heat shock. Exponentially growing cultures of wild-type, $\Delta set13$, $rpl42^{K55R}$, $rpl42^{P56Q}$, $\Delta gcn5$, and $\Delta gcn2$ cells growing in YEA were subjected to cold stress at 15 °C or heat shock at 48 °C for the times indicated. The total cell lysates prepared from the indicated strains were resolved on an 11% SDS-poly-acrylamide gel. The level of eIF2a phosphorylation was analyzed by immunoblotting using an antibody that specifically recognizes phosphorylated eIF2α (*top*). The Western blot signal of tubulin was used as a loading control (*bottom*).

activity and Rpl42 methylation correlate with the chronological life span.

DISCUSSION

Using an *in vitro* methyltransferase assay, we demonstrated that fission yeast Set13 is a methyltransferase for lysine 55 of the ribosomal protein Rpl42. Because under our assay conditions we could not detect any other proteins that were efficiently modified by Set13 (Fig. 1*B*), it is most likely that Rpl42 is a specific substrate for Set13. Although its direct enzymatic activity has yet to be examined, the budding yeast *SET7* gene was recently demonstrated to be required for the monomethylation at lysine 55 of Rpl42ab (16). In addition, we found that human Rpl36a/Rpl42 is also monomethylated at the corresponding lysine residue (Fig. 4). Together with a mass spectrometric analysis of plant ribosome proteins (19), these findings indicate that Rpl42/Rpl36a methylation and its responsible enzyme are highly conserved among a wide range of eukaryotic species.

In *S. cerevisiae*, Rpl42 is also monomethylated at lysine 40, and this methylation is dependent on the Ybr030w gene product (16). Although we could not obtain concrete evidence for a corresponding methylation in *S. pombe* Rpl42 or human Rpl36a (data not shown), a combination of methylation modifications at different residues on Rpl42 may modulate its function in certain species. Most of the methyl modifications on histones appear to be enzymatically reversed by a family of demethylases (5). It remains an open question whether a member of the demethylase family can target the methyl modifications on ribosomal proteins.

Because Rpl42 prepared from wild-type cells was not a good substrate for Set13 *in vitro* (Fig. 1*B*), it is likely that Rpl42 is predominantly methylated at lysine 55 in wild-type cells (16). In addition, Rpl42 is tightly associated with, or rather embedded in, the ribosomal RNA of the 60 S subunit (Fig. 5*B*). Rpl42 methylation appears to occur during the ribosomal assembly process, as supported by the nuclear localization of Set13 (Fig. 5*D*),

showing the more severe phenotype (Fig. 8, *A* and *B*). In contrast, the cycloheximide-resistant $rpl42^{P56Q}$ mutant cells exhibited a longer life span than wild-type cells (Fig. 8*A*). The survival potential appeared to correlate with cycloheximide sensitivity. Together, these results suggested that the Set13
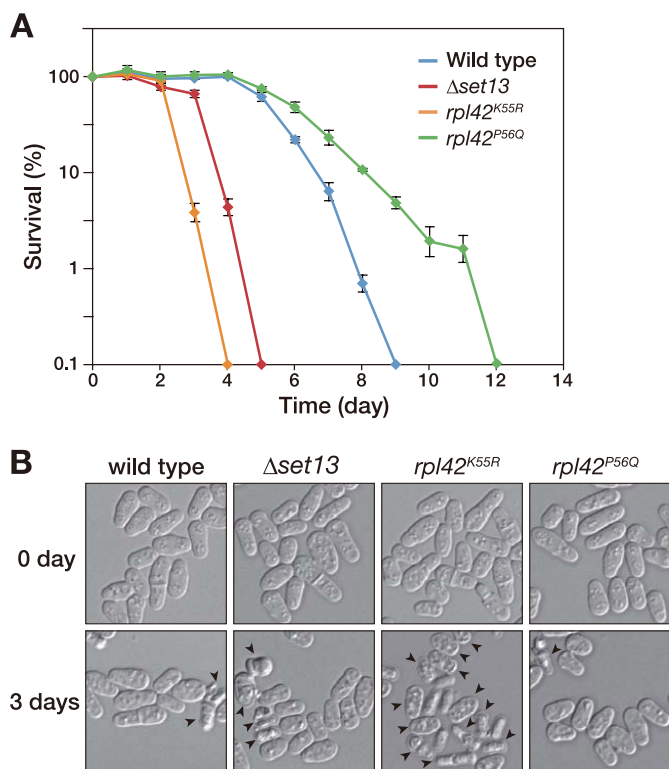
FIGURE 8. Rpl42 methylation and chronological life span. *A,* survival of wild-type, Δ*set13*, *rpl42*[K55A], and *rpl42*[P56Q] in stationary phase was evaluated by counting the colony-forming units. The *y* axis is shown in logarithmic scale. *B,* wild-type and mutant cells on the indicated days were observed under a light microscope. *Arrowheads* indicate abnormal or dead cells.

and once Rpl42 is assembled into the 60 S subunit, its methylation might be stably maintained and important for ribosomal function.

From the cryo-EM structure of the *S. cerevisiae* 80 S ribosome (42), Rpl42 was determined to lie close to the E-site (Fig. 5*B*). In addition, the x-ray crystal structure of complexes between the *H. marismortui* 50 S subunit and E-site substrates revealed that deacylated tRNA makes specific contacts with the loop extension of the L44e protein, the structural homologue of Rpl42, and the residues responsible for this interaction lie close to the region containing lysine 55 and proline 56 of Rpl42 (Fig. 5*C*) (43). Together, these observations support the possibility that the loop extension of Rpl42 and the methylation at lysine 55 play a critical role in an interaction with the deacylated tRNA positioned at the E-site. Intriguingly, human L36a-like, which is closely related to Rpl36a/Rpl42, has been demonstrated to make contact with the CCA end of P-site-bound tRNA (55). Therefore, it is also possible that Rpl42 plays a role in the recognition of tRNA positioned at the P-site.

The function of the E-site has been extensively studied for the *E. coli* ribosome. A specific interaction between the 3′ end of deacylated tRNA with the E-site is required for an efficient translocation reaction (56). Furthermore, the mutation of a highly conserved residue in the 23 S rRNA that interacts with the 3′ end of deacylated tRNA at the E-site leads to a translocation defect and promotes frameshifting and misreading at stop codons *in vivo* (57). According to these observations, we examined the efficiency of frameshifting events in the Δ*set13* and *rpl42* mutant cells. However, we could not obtain direct evidence for an

effect on frameshifting (data not shown). The role of E-site may be regulated differently in the eukaryotic ribosome.

The Δ*set13* and *rpl42*[K55R] mutant cells showed enhanced cycloheximide sensitivity, and in contrast, the *rpl42*[P56Q] mutant cells showed enhanced resistance to cycloheximide. Although the exact mechanism and the action site of this antibiotic have yet to be determined, these two residues and the methyl modification may affect the binding affinity of cycloheximide for the 60 S ribosome. This is quite consistent with a previous observation that cycloheximide arrests the ribosome when the first deacylated tRNA reaches the E-site (49).

It is noteworthy that the Δ*set13* and *rpl42* mutant cells also showed defects in stress-adapted growth control. Under stress or starvation conditions, translation initiation is blocked by eIF2α phosphorylation and eIF4F disassembly (22, 23). In this study, we demonstrated that the defects of the stress-induced growth control of Δ*set13* and *rpl42* mutant cells were distinct from the signaling pathways that control translation initiation.

Another intriguing finding was that the stress-adapted growth defect observed in these mutant cells appeared to be correlated, at least to some extent, with the cycloheximide sensitivity and chronological life span. As described above, a simple explanation for the cycloheximide sensitivity is that the loss of methylation or amino acid substitution at lysine 55 changes the structural conformation of Rpl42 in a way that affects the binding affinity of cycloheximide to the ribosome. However, this idea does not fully explain our observation that the cycloheximide sensitivity correlates with stress-adapted cell growth control.

It is conceivable that cycloheximide treatment mimics the condition of ribosomes under some sort of stress and that the methylation of Rpl42 at lysine 55 fine-tunes the ribosomal function rather than affecting the affinity of ribosome for cycloheximide. The loss of the methylation may lead to a defect in this precision machinery that results in a defect in the stress-responsive growth control. An alternative is that the E-site configuration determined by Rpl42 functions as an intrinsic sensor of environmental conditions and modulates ribosomal function. In this scenario, the Δ*set13* and *rpl42* mutant cells would be defective in their ability to sense environmental conditions or to change the growth rate to the appropriate level.

Some yeast species possess a variant Rpl42 that confers cycloheximide resistance on the cell (58). It is possible that cells adapt to stress by preparing several subtypes of ribosomes that provide distinct responses to environmental stresses. It is interesting to imagine that a minor fraction of ribosomes that contains unmodified Rpl42 plays a role under stress conditions and affects cellular processes such as cancer development in humans (59). Further studies are necessary to elucidate how methylation of Rpl42 regulates stress-adapted cell growth.

Rpl42 Methylation Regulates Ribosomal Function

REFERENCES

1. Clarke, S. G., and Tamanoi, F. (eds) (2006) *The Enzymes,* 3rd Ed., Vol. 24, Academic Press, San Diego
2. Qian, C., and Zhou, M. M. (2006) *Cell. Mol. Life Sci.* **63,** 2755–2763
3. Lachner, M., and Jenuwein, T. (2002) *Curr. Opin. Cell Biol.* **14,** 286–298
4. Martin, C., and Zhang, Y. (2005) *Nat. Rev. Mol. Cell Biol.* **6,** 838–849
5. Klose, R. J., and Zhang, Y. (2007) *Nat. Rev. Mol. Cell Biol.* **8,** 307–318
6. Houtz, R. L., and Portis, A. R., Jr. (2003) *Arch. Biochem. Biophys.* **414,** 150–158
7. Polevoda, B., Martzen, M. R., Das, B., Phizicky, E. M., and Sherman, F. (2000) *J. Biol. Chem.* **275,** 20508–20513
8. Kouskouti, A., Scheer, E., Staub, A., Tora, L., and Talianidis, I. (2004) *Mol. Cell* **14,** 175–182
9. Chuikov, S., Kurash, J. K., Wilson, J. R., Xiao, B., Justin, N., Ivanov, G. S., McKinney, K., Tempst, P., Prives, C., Gamblin, S. J., Barlev, N. A., and Reinberg, D. (2004) *Nature* **432,** 353–360
10. Huang, J., Perez-Burgos, L., Placek, B. J., Sengupta, R., Richter, M., Dorsey, J. A., Kubicek, S., Opravil, S., Jenuwein, T., and Berger, S. L. (2006) *Nature* **444,** 629–632
11. Polevoda, B., and Sherman, F. (2007) *Mol. Microbiol.* **65,** 590–606
12. Lhoest, J., Lobet, Y., Costers, E., and Colson, C. (1984) *Eur. J. Biochem.* **141,** 585–590
13. Lee, S. W., Berger, S. J., Martinoviæ, S., Pasa-Toliæ, L., Anderson, G. A., Shen, Y., Zhao, R., and Smith, R. D. (2002) *Proc. Natl. Acad. Sci. U.S.A.* **99,** 5942–5947
14. Porras-Yakushi, T. R., Whitelegge, J. P., Miranda, T. B., and Clarke, S. (2005) *J. Biol. Chem.* **280,** 34590–34598
15. Porras-Yakushi, T. R., Whitelegge, J. P., and Clarke, S. (2006) *J. Biol. Chem.* **281,** 35835–35845
16. Webb, K. J., Laganowsky, A., Whitelegge, J. P., and Clarke, S. G. (2008) *J. Biol. Chem.* **283,** 35561–35568
17. Odintsova, T. I., Müller, E. C., Ivanov, A. V., Egorov, T. A., Bienert, R., Vladimirov, S. N., Kostka, S., Otto, A., Wittmann-Liebold, B., and Karpova, G. G. (2003) *J. Protein Chem.* **22,** 249–258
18. Yu, Y., Ji, H., Doudna, J. A., and Leary, J. A. (2005) *Protein Sci.* **14,** 1438–1446
19. Carroll, A. J., Heazlewood, J. L., Ito, J., and Millar, A. H. (2008) *Mol. Cell. Proteomics* **7,** 347–369
20. VanBogelen, R. A., and Neidhardt, F. C. (1990) *Proc. Natl. Acad. Sci. U.S.A.* **87,** 5589–5593
21. Ashe, M. P., De Long, S. K., and Sachs, A. B. (2000) *Mol. Biol. Cell* **11,** 833–848
22. Holcik, M., and Sonenberg, N. (2005) *Nat. Rev. Mol. Cell Biol.* **6,** 318–327
23. Sonenberg, N., and Hinnebusch, A. G. (2009) *Cell* **136,** 731–745
24. Aguilera, J., Randez-Gil, F., and Prieto, J. A. (2007) *FEMS Microbiol. Rev.* **31,** 327–341
25. Steffen, K. K., MacKay, V. L., Kerr, E. O., Tsuchiya, M., Hu, D., Fox, L. A., Dang, N., Johnston, E. D., Oakes, J. A., Tchao, B. N., Pak, D. N., Fields, S., Kennedy, B. K., and Kaeberlein, M. (2008) *Cell* **133,** 292–302
26. Curran, S. P., and Ruvkun, G. (2007) *PLoS Genet.* **3,** e56
27. Chen, D., Pan, K. Z., Palter, J. E., and Kapahi, P. (2007) *Aging Cell* **6,** 525–533
28. Hansen, M., Taubert, S., Crawford, D., Libina, N., Lee, S. J., and Kenyon, C. (2007) *Aging Cell* **6,** 95–110
29. Nakayama, J., Rice, J. C., Strahl, B. D., Allis, C. D., and Grewal, S. I. (2001) *Science* **292,** 110–113
30. Noma, K., and Grewal, S. I. (2002) *Proc. Natl. Acad. Sci. U.S.A.* **99,** Suppl. 4, 16438–16445
31. Morris, S. A., Shibata, Y., Noma, K., Tsukamoto, Y., Warren, E., Temple, B., Grewal, S. I., and Strahl, B. D. (2005) *Eukaryot. Cell* **4,** 1446–1454
32. Sanders, S. L., Portoso, M., Mata, J., Bähler, J., Allshire, R. C., and Kouzarides, T. (2004) *Cell* **119,** 603–614
33. Shirai, A., Matsuyama, A., Yashiroda, Y., Hashimoto, A., Kawamura, Y., Arai, R., Komatsu, Y., Horinouchi, S., and Yoshida, M. (2008) *J. Biol. Chem.* **283,** 10745–10752
34. Sadaie, M., Shinmyozu, K., and Nakayama, J. (2008) *J. Biol. Chem.* **283,** 7185–7195
35. Krawchuk, M. D., and Wahls, W. P. (1999) *Yeast* **15,** 1419–1427
36. Sadaie, M., Iida, T., Urano, T., and Nakayama, J. (2004) *EMBO J.* **23,** 3825–3835
37. Matsuyama, A., Arai, R., Yashiroda, Y., Shirai, A., Kamata, A., Sekido, S., Kobayashi, Y., Hashimoto, A., Hamamoto, M., Hiraoka, Y., Horinouchi, S., and Yoshida, M. (2006) *Nat. Biotechnol.* **24,** 841–847
38. Matsuyama, A., Shirai, A., Yashiroda, Y., Kamata, A., Horinouchi, S., and Yoshida, M. (2004) *Yeast* **21,** 1289–1305
39. Ekwall, K., Olsson, T., Turner, B. M., Cranston, G., and Allshire, R. C. (1997) *Cell* **91,** 1021–1032
40. Lyne, R., Burns, G., Mata, J., Penkett, C. J., Rustici, G., Chen, D., Langford, C., Vetrie, D., and Bähler, J. (2003) *BMC Genomics* **4,** 27
41. Ban, N., Nissen, P., Hansen, J., Moore, P. B., and Steitz, T. A. (2000) *Science* **289,** 905–920
42. Spahn, C. M., Gomez-Lorenzo, M. G., Grassucci, R. A., Jørgensen, R., Andersen, G. R., Beckmann, R., Penczek, P. A., Ballesta, J. P., and Frank, J. (2004) *EMBO J.* **23,** 1008–1019
43. Schmeing, T. M., Moore, P. B., and Steitz, T. A. (2003) *RNA* **9,** 1345–1352
44. Käufer, N. F., Fried, H. M., Schwindinger, W. F., Jasin, M., and Warner, J. R. (1983) *Nucleic Acids Res.* **11,** 3123–3135
45. Roguev, A., Wiren, M., Weissman, J. S., and Krogan, N. J. (2007) *Nat. Methods* **4,** 861–866
46. Borovinskaya, M. A., Pai, R. D., Zhang, W., Schuwirth, B. S., Holton, J. M., Hirokawa, G., Kaji, H., Kaji, A., and Cate, J. H. (2007) *Nat. Struct. Mol. Biol.* **14,** 727–732
47. Borovinskaya, M. A., Shoji, S., Fredrick, K., and Cate, J. H. (2008) *RNA* **14,** 1590–1599
48. Blaha, G., Gürel, G., Schroeder, S. J., Moore, P. B., and Steitz, T. A. (2008) *J. Mol. Biol.* **379,** 505–519
49. Pestova, T. V., and Hellen, C. U. (2003) *Genes Dev.* **17,** 181–186
50. Dunand-Sauthier, I., Walker, C. A., Narasimhan, J., Pearce, A. K., Wek, R. C., and Humphrey, T. C. (2005) *Eukaryot. Cell* **4,** 1785–1793
51. Ma, X. M., and Blenis, J. (2009) *Nat. Rev. Mol. Cell Biol.* **10,** 307–318
52. Vivancos, A. P., Jara, M., Zuin, A., Sansó, M., and Hidalgo, E. (2006) *Mol. Genet. Genomics* **276,** 495–502
53. Fabrizio, P., Pozza, F., Pletcher, S. D., Gendron, C. M., and Longo, V. D. (2001) *Science* **292,** 288–290
54. Roux, A. E., Quissac, A., Chartrand, P., Ferbeyre, G., and Rokeach, L. A. (2006) *Aging Cell* **5,** 345–357
55. Baouz, S., Woisard, A., Sinapah, S., Le Caer, J. P., Argentini, M., Bulygin, K., Aguié, G., and Hountondji, C. (2009) *Biochimie* **91,** 1420–1425
56. Lill, R., Robertson, J. M., and Wintermeyer, W. (1989) *EMBO J.* **8,** 3933–3938
57. Sergiev, P. V., Lesnyak, D. V., Kiparisov, S. V., Burakovsky, D. E., Leonov, A. A., Bogdanov, A. A., Brimacombe, R., and Dontsova, O. A. (2005) *Nucleic Acids Res.* **33,** 6048–6056
58. Takaku, H., Mutoh, E., Sagehashi, Y., Fukuda, R., Horiuchi, H., Ochi, K., Takagi, M., and Ohta, A. (2004) *J. Biol. Chem.* **279,** 23030–23037
59. Kim, J. H., You, K. R., Kim, I. H., Cho, B. H., Kim, C. Y., and Kim, D. G. (2004) *Hepatology* **39,** 129–138